Available online at www.sciencedirect.com
ScienceDirect
Ceramics International 35 (2009) 2305–2310
CERAMICS INTERNATIONAL
www.elsevier.com/locate/ceramint

Formation of rod-like Si_3N_4 grains in porous SRBSN bodies using $6Y_2O_3$–2MgO sintering additives

Do-Van Tuyen [a,b], Young-Jo Park [c], Hai-Doo Kim [c], Byong-Taek Lee [a,*]

[a] Department of Biomedical Engineering and Materials, Soonchunhyang University, 366-1 Ssangyong-dong, Cheonan, Chungnam 330-090, South Korea
[b] Department of Display Materials Engineering, Soonchunhyang University, Asan, Chungnam 336-745, South Korea
[c] Ceramic Materials Group, Korea Institute of Materials Science, Changwon, Kyungnam 641-010, South Korea

Received 27 November 2008; received in revised form 14 December 2008; accepted 12 January 2009
Available online 6 February 2009

Abstract

The porous reaction-bonded silicon nitride (RBSN) bodies using (6 wt.% Y_2O_3–2 wt.% MgO) 6Y2M were fabricated by nitridation process at 1350 °C for 8 h. The porous gas pressure sintered (GPSed)-RBSN bodies post-sintered at 1550–1850 °C for 6 h show a microstructure with low aspect ratios having high porosity. The compressive strength of samples sintered at 1650 °C, 1750 °C and 1850 °C were about 146 MPa, 251 MPa and 285 MPa, respectively. The duration time for sintering had a significant effect on the microstructure and grain morphology of the GPSed-RBSN bodies. Even though the GPSed-RBSN was carried out at the comparatively low temperature (1550 °C) for 9 h, high aspect ratio of rod-like Si_3N_4 grains with about 9 was observed. The material properties of samples such as porosity, phase ratio ($\beta/(\alpha+\beta)$) and compressive strength of sample sintered at 9 h were about 43.2%, 99% and 141 MPa, respectively.

Keywords: A. Grain growth; B. Porosity; D. Si_3N_4; RBSN

1. Introduction

Recently, porous silicon nitride ceramics have been actively investigated for use as environmental filters for the purification of polluted air, water and hot gases, separation membranes and catalyst supports [1–4]. Furthermore, silicon nitride has some advantages such as superior mechanical properties at both room temperature and high temperatures. Thus, porous Si_3N_4 has potential for use as an engineering material and some processes have been developed to produce porous Si_3N_4 ceramics [2–4]. It is known that using α-Si_3N_4 powder with different sintering additives to produce porous silicon nitride ceramics results in high grain aspect ratios, superior mechanical properties and strain tolerance [1,5]. However, due to the high cost of α-Si_3N_4 powder, reaction-bonded silicon nitride (RBSN) is a candidate material for investigation due to its low cost. That can be made by a direct nitridation process using a Si powder compact for its advantages of the low price of raw Si powder, easy control of dimensions, low cost of production, and good thermal and chemical stability at high temperatures [6,7]. In addition, the needle-shaped grains of β-Si_3N_4 in the porous Si_3N_4 ceramics can be beneficial to improve the surface area while maintaining the desired mechanical properties.

In general, the sintering of Si_3N_4 ceramics is difficult because of strong covalent bonding between silicon and nitrogen atoms [8]. The densification of Si_3N_4 ceramics requires sintering additives and proceeds through a liquid-phase sintering mechanism. With the aid of metal oxide sintering additives such as MgO, Al_2O_3, Y_2O_3 and other rare earth oxides, such as Yb_2O_3, Dy_2O_3, etc. or their combinations as Y_2O_3–Al_2O_3, Yb_2O_3–MgO, dense and porous Si_3N_4 ceramics have been produced [1,5,9–12]. Some authors have reported the fabrication and mechanical properties of porous Si_3N_4 ceramics using the sintering additives such as Yb_2O_3 or RE_2O_3–MgO–(CaO) (where RE = (La, Nd, Y or Yb)) with different content [1,5]. By choosing suitable fabrication conditions, the porous silicon nitride ceramics have a high porosity (40–60%) with superior mechanical properties [5]. There are already many reports about using MgO combined with other oxides such as Y_2O_3, Yb_2O_3, La_2O_3, etc. as sintering additives for the

* Corresponding author. Tel.: +82 41 570 2427; fax: +82 41 577 2415.
E-mail address: lbt@sch.ac.kr (B.-T. Lee).

0272-8842/$34.00
doi:10.1016/j.ceramint.2009.01.010

densification of Si_3N_4 with a high aspect ratio. However, most of them were used for sintering at relatively high temperatures, between 1700 °C and 1900 °C [1,10,13], and using raw Si_3N_4 powder to produce bulk ceramic bodies gives rise to a high cost for production. That is a major barrier in limiting the widespread application of Si_3N_4 ceramic components.

The diesel particulate filter (DPF) made with ceramics has been used in order to reduce diesel particulate matter (PM) emissions in the automotive area. Among these ceramic materials, Si_3N_4 is also a material candidate for the DPF [14]. The DPF substrate needs to have excellent thermal shock resistance, and thermal and chemical stability. However, a DPF having a high surface area as well as the desired mechanical strength has always been considered important to improve the filtration efficiency. When porosity is increased and the pore-surface of a DPF modified, the filtration efficiency can be further increased.

In the present work, the porous RBSN bodies using 6 wt.% Y_2O_3–2 wt.% MgO (6Y2M) sintering additives were fabricated by post-sintering at a remarkably low sintering temperature (1550 °C) using gas pressure sintering (GPSed-RBSN) depending on the sintering time. The sintered samples were characterized in terms of crystalline phases, phase ratio, microstructures and mechanical properties. The morphology of the needle-shaped β-Si_3N_4 grains was analyzed depending especially on the post-sintering temperature and duration of sintering.

2. Experimental procedure

Porous GPSed-RBSN is fabricated from commercial Si powder (average particle size: 7 μm, Permascand, Sweden, BET: 1.2 m^2/g) using PMMA powder (average particle size diameter: 20 μm, Aldrich, Japan) as a pore-forming agent.

As the sintering additive, 6 wt.% Y_2O_3 (purity > 99.9%, Aldrich, USA)–2 wt.% MgO (purity > 99.9%, Aldrich, USA) were mixed with Si powders and 20 wt.% PMMA powders using a wet ball mill in alcohol for 12 h using Si_3N_4 ball as a milling media. The slurry was separated from the milling media and dried on a hot plate while stirring. The mixture was then kept in the oven at 60 °C for 24 h. After that, it was compacted by uniaxial pressing to make the disk shape having a diameter of about 31 mm. The burn-out of samples was performed at 600 °C for 1 h in an air atmosphere to remove the PMMA. After the burn-out, the samples were nitrided in a flowing N_2–10% H_2 gas mixture at 1350 °C for 8 h to fabricate porous RBSN ceramics. To improve the mechanical properties of RBSN, the samples were embedded in the mixture powder (50 wt.% Si_3N_4 + 50 wt.% BN) at different temperatures (1550–1850 °C) for 6 h under 5 MPa nitrogen gas pressure.

The porous RBSN and GPSed-RBSN samples were crushed into a powder and were analyzed to identify the phase composition using X-ray diffraction (XRD, D/MAX-250, Rigaku, Japan). The porosity of porous RBSN and GPSed-RBSN bodies was measured by the Archimedes method. The microstructure of the porous RBSN and GPSed-RBSN bodies was observed by scanning electron microscopy (SEM, JSM-635F, Jeol). The phase ratio $\beta/(\alpha + \beta)$ Si_3N_4 of the fabricated porous bodies was calculated from the XRD profiles on the basis of α-Si_3N_4 and β-Si_3N_4 peak intensities as reported by the Gazzara and Messier equation [15]. The compressive strength measurement was carried out using a universal testing machine (Unitech TM, R&B, Korea).

3. Results and discussion

Fig. 1 shows (a) low magnification of a SEM polished surface and (b) high magnification of the fracture surface of the porous GPSed-RBSN using 6Y2M sintering additive at 1550 °C for 6 h. The GPSed-RBSN body as shown in Fig. 1(a) shows the porous structures due to the removal of the pore-forming agent PMMA as shown with dotted circles during the burning out process at 600 °C in an air atmosphere. On the other hand, in Fig. 1(b), the SEM micrograph of fracture surface exhibits a typical microstructure of GPSed-RBSN porous microstructure with pores which were homogeneously distributed in the sintered RBSN body ceramics with the average size of about 2 μm in diameter, as shown by the dotted circles. The formation of pores on the microstructure is due to the low viscosity of the 6Y2M sintering additives. This is explained in a previous report [9]. Further, the microstructure of the sample shows fine elongated Si_3N_4 grains only and unimodal grain size distribution. The average diameter and elongation of the rod-like Si_3N_4 grains were about 0.35 μm and 1.5 μm, respectively.

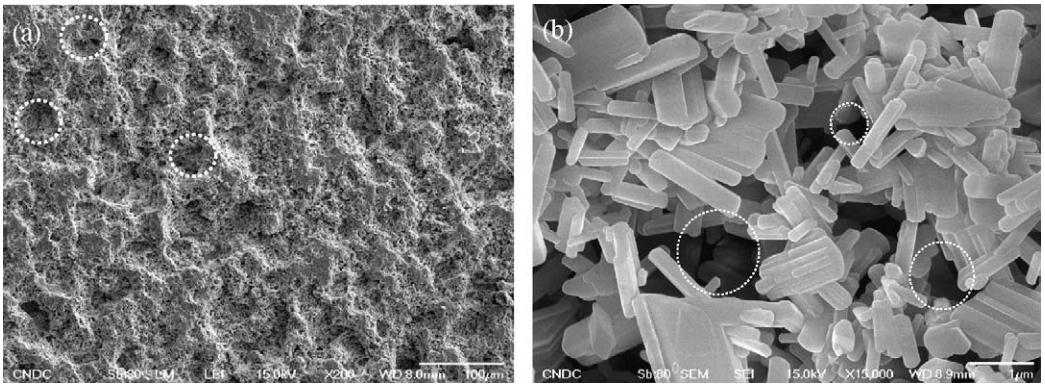

Fig. 1. (a) Low and (b) high magnification SEM micrographs of the porous SRBSN bodies using 6Y2M sintering additive sintered at 1550 °C for 6 h.

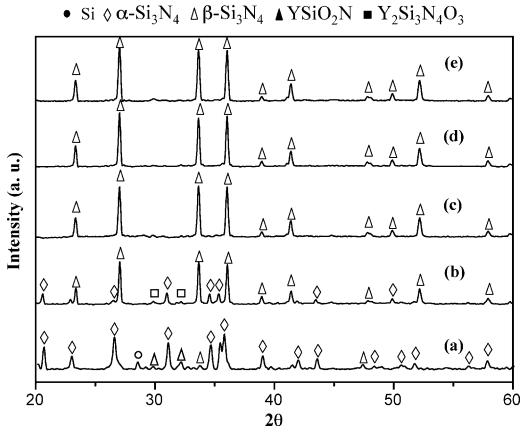

Fig. 2. XRD profiles of the porous SRBSN bodies using 6Y2M sintering additive nitrided at (a) 1350 °C for 8 h and sintered at (b) 1550 °C, (c) 1650 °C, (d) 1750 °C and 1850 °C for 6 h.

Fig. 2 shows XRD profiles of the porous bodies depending on the sintering temperature. From XRD profiles of nitrided samples as shown in Fig. 2(a) both α- and β-Si_3N_4 were formed with the major α-Si_3N_4 together with minor β-Si_3N_4 and residual Si peaks. The $YSiO_2N$ phase was also observed. The formation of this crystalline secondary phase was reported by Zhu et al. [10] and Kleebe and Ziegler [16]. On the other hand, no crystalline secondary phase containing Mg was detected by XRD at 1350 °C. This can be explained, in that, similar to Al_2O_3, MgO takes part in the formation of a liquid phase to form an amorphous grain-boundary phase [17]. It has also been reported that the lowest eutectic temperature of the Si_3N_4–SiO_2–Y_2O_3–MgO does not exceed 1350 °C [10]. When the sintering temperature was increased to 1550 °C, no Si peaks were observed in the XRD profiles while the intensities of α-Si_3N_4 phase gradually decreased and the intensities of β-Si_3N_4 increased as shown in Fig. 2(b). However, the appearance of the $Y_2Si_3N_4O_3$ phase at this sintering temperature was due to the change of the crystalline secondary phase from $YSiO_2N$ to $Y_2Si_3N_4O_3$. That phase was not observed as the sintering temperature was increased up to 1650 °C and beyond. At these sintering temperatures, α-Si_3N_4 was almost completely transformed into β-Si_3N_4 while the $Y_2Si_3N_4O_3$ phase was not detected, perhaps due to the formation of an amorphous phase.

Fig. 3 shows SEM fracture surfaces of the porous GPSed-RBSN bodies depending on the sintering temperatures for 6 h. The microstructure of the sample sintered at 1550 °C shows fine, rod-like β-Si_3N_4 grains, while some of the α-Si_3N_4 grains still were not transformed to β-Si_3N_4, as indicated by the round grains marked by arrowheads in Fig. 3(a). This is confirmed by XRD analysis in Fig. 2(b). Furthermore, in the porous microstructure, a number of pores were also observed with an average size of about 1–2 μm in diameter, as shown by the dotted circle. When the sintering temperature was increased to 1650 °C, the microstructure showed that the diameter and aspect ratio of elongated β-Si_3N_4 grains were not significantly changed compared with grains sintered at 1550 °C. From

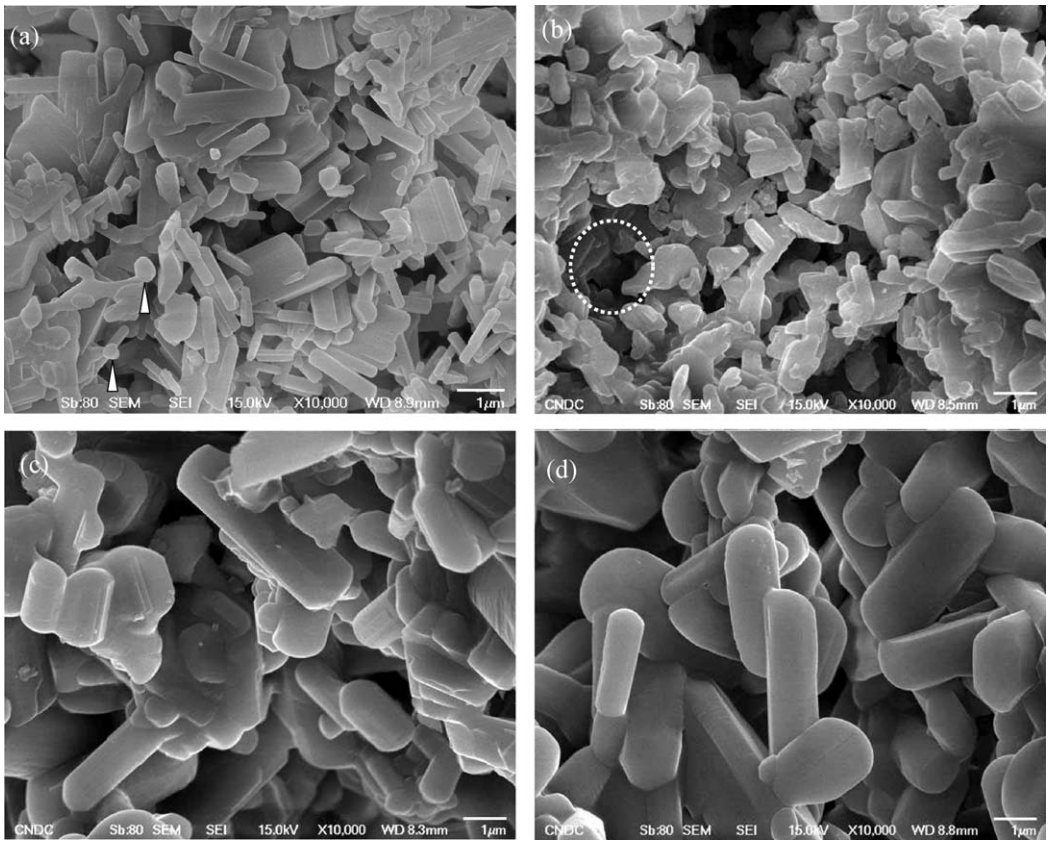

Fig. 3. SEM micrographs of the porous SRBSN bodies using 6Y2M sintering additive sintered at (a)1550 °C, (b)1650 °C, (c)1750 °C and (d)1850 °C for 6 h.

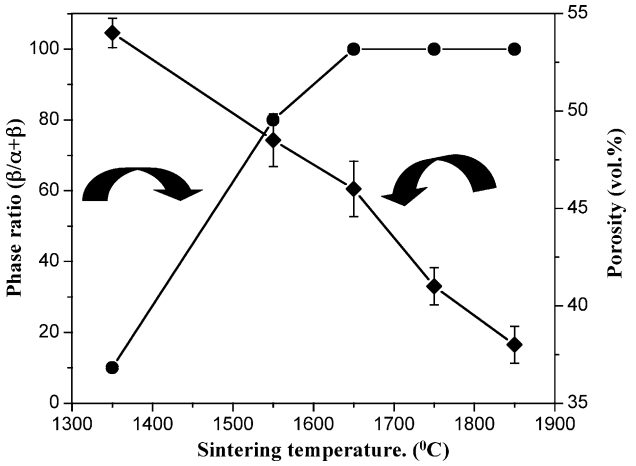

Fig. 4. Phase ratio (β/(α + β)) and porosity of the porous SRBSN bodies using 6Y2M sintering additive depending on the different sintering temperatures for 6 h.

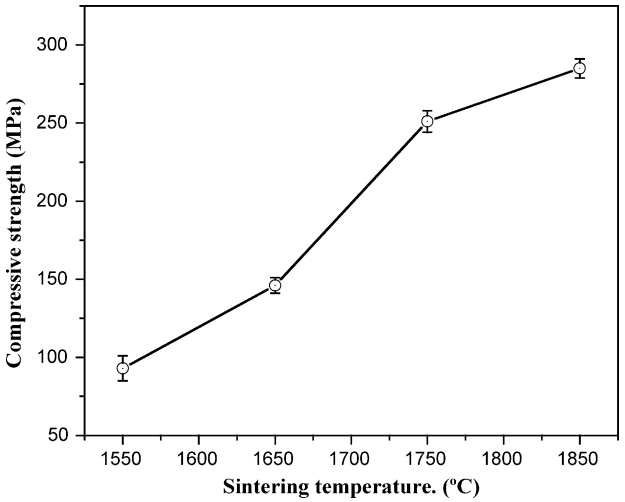

Fig. 5. Compressive strength of the porous SRBSN bodies using 6Y2M sintering additive depending on the sintering temperatures for 6 h.

Fig. 2(c), the XRD profile shows that the appearance of the Si_3N_4 grains was almost the same as for β-Si_3N_4. As a result, at this sintering temperature only the phase transformation occurred without any significant change in grain morphology. When the samples were sintered at 1750 °C and 1850 °C, the microstructure with coarse grains where both the length and diameter of the rod-like β-Si_3N_4 grains increased was obtained. However, although the increase of grain size is remarkable, the aspect ratio was not increased significantly compared to that sintered at 1550 °C and 1650 °C. It is understood that the available liquid phase due to Y_2O_3 acts as a sintering aid to accelerate the α- to β-phase and grain growth via the dissolution–reprecipitation that was reported by some authors [18–20]. Furthermore, XRD profiles in Fig. 2(c) show that when sintering was done at 1650 °C, the secondary phase was not observed, which suggests that the growth of β-Si_3N_4 grains took place at lower viscosity at higher temperatures. Hence, the aspect ratio of elongated grains is the same at sintering temperatures of 1750 °C and 1850 °C, although the grain size increased minimally at 1850 °C.

Fig. 4 shows phase ratio (β/(α + β)) and porosity of the porous GPSed-RBSN bodies sintered at different sintering temperatures. It shows the relationship between porosity and sintering temperatures. The change in the porosity was a linear function of the sintering temperature. The phase ratio of the ceramics depending on sintering temperature is also shown. However, when the samples were sintered at 1550 °C, it led to decreased porosity due to the growth of β-Si_3N_4 grains and the porosity and phase ratio were about 48.5% and 80%, respectively. Furthermore, the phase ratio was 100% as the sintering temperature increased up to 1650 °C and beyond, while the porosity gradually decreased. The minimum value of the porosity was about 38% when sintered at 1850 °C.

Fig. 5 shows the compressive strength of the porous GPSed-RBSN bodies depending on the sintering temperature for 6 h. The relation between compressive strength and sintering temperatures is seen as almost linear. In the sample sintered at 1550 °C, the value of the compressive strength was 93 MPa. However, as the sintering temperature increased, the values of compressive strength increased due to growth of rod-like β-Si_3N_4 grains. At 1850 °C, the maximum compressive strength of 285 MPa was obtained.

Fig. 6 shows SEM fracture surfaces of the porous GPSed-RBSN bodies sintered at 1550 °C for 3 h and 9 h, respectively.

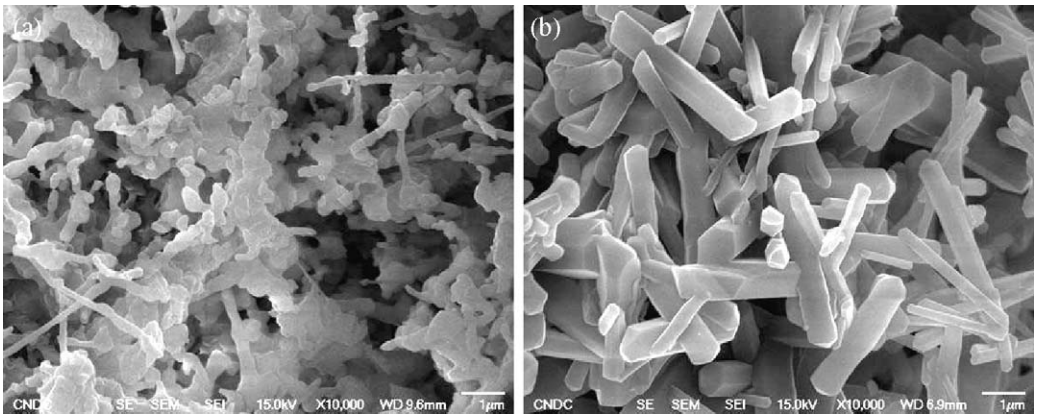

Fig. 6. SEM micrographs of fracture surfaces of the porous SRBSN bodies sintered at 1550 °C for (a) 3 h and (b) 9 h.

Fig. 6(a) shows very fine Si_3N_4 whiskers with a high aspect ratio and a few rod-like β-Si_3N_4 in an agglomerated form. The average diameter of Si_3N_4 whiskers was about 200 nm. From Moulson's proposal [21], it is believed that the major growth of the β-phase occurs in the liquid phase and the growth of the α-phase occurs by vapor-phase reactions. This suggests that the formation of the whiskers may be due to the vapor phase reaction between SiO and N_2 gas during nitridation. The formation of the intermediate SiO phase was possible because the reaction between SiO_2 formed at the surface of the starting Si powder and H_2 in the gas mixture occurred in the early stage of nitridation ($SiO_2 + H_2 \rightarrow SiO_{(g)} + H_2O_{(g)}$). SiO gas reacted with N_2 gas to form α-Si_3N_4 whiskers following the reaction ($3SiO_{(g)} + 2N_{2(g)} \rightarrow \alpha\text{-}Si_3N_4 + (3/2)O_2$) and the formation α-$Si_3N_4$ was previously reported [22]. On the other hand, the formation of α-Si_3N_4 whiskers was also reported by VLS process due to SiO vapor supply to the liquid droplet that was present on the tip of the growing whisker [23]. When the sintering time is increased to 6 h, the matrix contains fine rod-like β-Si_3N_4 grains. Increasing the sintering time caused the formation and development of β-Si_3N_4 grains, indicating enhanced phase transformation as shown in Fig. 7 and grain growth as shown in Fig. 3(a). Furthermore, when the sintering time was 9 h, the β-Si_3N_4 grains grew mostly in length, with large elongated grains. The matrix grains are randomly oriented with the average diameter and length of the grains being about 0.43 μm and 4.0 μm, respectively, as shown in Fig. 6(b). The growth of rod-like β-Si_3N_4 grains can be explained as being due to the available liquid phase to promote grain growth. XRD profiles as shown in Fig. 7 show that the secondary phase exists in the body sintered at 1550 °C and the eutectic point of the Y_2O_3–SiO_2–Si_3N_4 system is below 1630 °C as reported by Kitayama et al. [20]. Therefore, a Y–Si–O–N liquid was able to be formed and is beneficial for the α- to β-phase transformation and elongated β-Si_3N_4 grains.

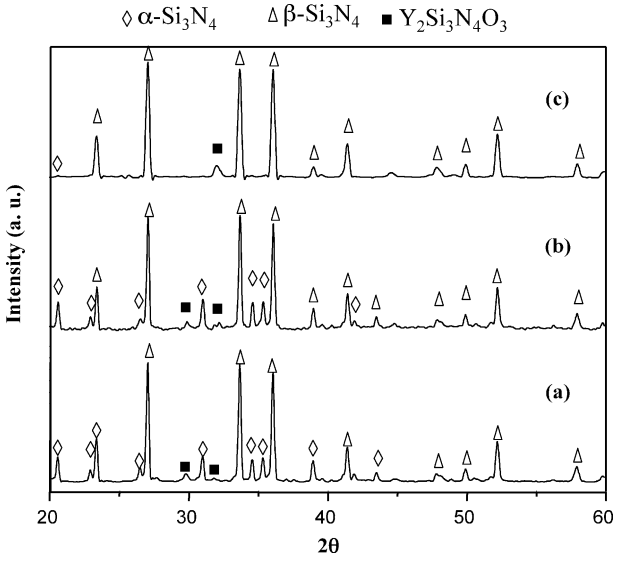

Fig. 7. XRD patterms of the porous SRBSN sintered at 1550 °C for (a) 3 h, (b) 6 h and (c) 9 h.

Table 1
Material properties of the porous SRBSN bodies at 1550 °C depending on the sintering time.

Properties	Time		
	3 h	6 h	9 h
Porosity (vol.%)	51	48.5	43.2
Phase ratio (β/(α + β))	75	80	99
Compressive strength (MPa)	81	93	141

Fig. 7 shows XRD profiles of the porous GPSed-RBSN bodies sintered at 1550 °C depending on the sintering time of 3 h, 6 h and 9 h. For 3 h sintering time, no Si peaks are detected while in the sintering for 9 h, almost all of the α-Si_3N_4 peaks had been transformed into β-Si_3N_4 and the crystalline secondary phase $Y_2Si_3N_4O_3$ still existed with lower intensity after sintering.

Table 1 gives material properties of porous GPSed-RBSN bodies sintered at 1550 °C depending on the different sintering times. It shows the porosity, phase ratio β/(α + β) and compressive strength as a function of the sintering time. When the sintering time increases, the porosity decreases, while the phase ratio and compressive strength increase. At a sintering time of 9 h, the material possesses maximum values of compressive strength and phase ratio β/(α + β), and a minimum value of porosity with 141 MPa, 99% and 43.2%, respectively.

4. Conclusions

Porous GPSed-RBSN bodies were successfully fabricated by gas pressure sintering depending on different sintering temperatures (1550–1850 °C) for 6 h and different sintering times (3–9 h) at 1550 °C under a nitrogen pressure using 6Y2M sintering additives. The effect of sintering time on the microstructure for elongated β-Si_3N_4 grains having fine matrix grains with a high aspect ratio at a low sintering temperature (1550 °C) for 9 h was found. The average diameter and elongated grains of the porous body were about 0.43 μm and 4.0 μm, respectively. The phase ratio β/(α + β), porosity and compressive strength of the porous GPSed-RBSN bodies were 99%, 43.2% and 141 MPa, respectively, while the maximum values of compressive strength and porosity of the porous GPSed-RBSN bodies, which were sintered at 1850 °C for 6 h, were about 285 MPa and 38%, respectively. The average diameter of the β-Si_3N_4 grains and elongated grains were about 1 μm and 4 μm, respectively.

References

[1] K.P. Plucknett, M. Quinlan, L. Garrido, L. Genova, Microstructural development in porous β-Si_3N_4 ceramics prepared with low volume RE_2O_3–MgO–(CaO) additions (RE = La, Nd, Y, Yb), Mater. Sci. Eng. A 489 (2008) 337–350.
[2] Y. Inagaki, T. Ohji, S. Kanzaki, Y. Shigegaki, Fracture energy of an aligned porous silicon nitride, J. Am. Ceram. Soc. 83 (2000) 1807–1809.
[3] G.J. Zhang, J.F. Yang, T. Ohji, Fabrication of porous ceramics with unidirectionally aligned continuous pores, J. Am. Ceram. Soc. 84 (6) (2001) 1395–1397.

[4] J.F. Yang, G.J. Zhang, T. Ohji, Porosity and microstructure control of porous ceramics by partial hot-pressing, J. Mater. Res. 16 (7) (2001) 1916–1918.
[5] J.F. Yang, Z.Y. Deng, T. Ohji, Effect of the addition of β-Si_3N_4 nuclei on the thermal conductivity of β-Si_3N_4 ceramics, J. Eur. Ceram. Soc. 23 (2003) 371–378.
[6] J.C. Bressiani, V. Izhevskyi, A.H.A. Bressiant, Development of the microstructure of the silicon nitride based ceramics, Mater. Res. 2 (1999) 165–172.
[7] B.T. Lee, R.K. Paul, C.W. Lee, H.D. Kim, Fabrication and microstructure characterization of continuously porous Si_2N_2O–Si_3N_4 ceramics, Mater. Lett. 61 (2007) 2182–2186.
[8] C.M. Wang, X.Q. Pan, M. Rühle, F.L. Riley, M. Mitomo, Silicon nitride crystal structure and observations of lattice defects, J. Mater. Sci. 31 (1996) 203–209.
[9] B.T. Lee, H.K. Kim, Effect of additives on the nitridation behaviour of reaction-bonded silicon nitride, Mater. Sci. Eng. A 364 (2004) 126–131.
[10] X. Zhu, Y. Zhou, K. Hirao, Effects of processing method and additive composition on microstructure and thermal conductivity of Si_3N_4 ceramics, J. Eur. Ceram. Soc. 26 (2006) 711–718.
[11] H.H. Lu, J.L. Huang, Effect of Y_2O_3 and Yb_2O_3 on the microstructure and mechanical properties of silicon nitride, Ceram. Int. 27 (2001) 621–628.
[12] Y. Goto, G. Thomas, Microstructure of silicon nitride ceramics sintered with rare-earth oxides, Acta Metall. Mater. 43 (3) (1995) 923–930.
[13] X. Zhu, Y. Zhou, K. Hirao, Effect of sintering additive composition on the processing and thermal conductivity of sintered reaction-bonded Si_3N_4, J. Am. Ceram. Soc. 87 (7) (2006) 1398–1400.
[14] J. Adler, Ceramic diesel particulate filters, J. Appl. Ceram. Technol. 2 (6) (2005) 429–439.
[15] C.P. Gazzara, D.R. Messier, Determination of phase content of Si_3N_4 by X-ray diffraction analysis, Am. Ceram. Bull. 56 (9) (1977) 777–780.
[16] H.J. Kleebe, G. Ziegler, Influence of crystalline secondary phases on densification of reaction-bonded silicon nitride during post sintering under increased nitrogen pressure, J. Am. Ceram. Soc. 72 (1989) 2314–2317.
[17] L.K.L. Falk, R. Pompe, G.L. Bunlop, Development of microstructure during the fabrication of Si_3N_4 by nitridation and pressureless sintering of Si:Si_3N_4 compacts, J. Mater. Sci. 20 (1985) 3545–3556.
[18] K. Watari, K. Hirao, M. Toriya, Effect of grain size on the thermal conductivity of Si_3N_4, J. Am. Ceram. Soc. 82 (3) (1999) 777–779.
[19] M. Katayama, K. Hirao, A. Tsuge, K. Watari, M. Toriyama, S. Kanzaki, Thermal conductivity of β-Si_3N_4: effect of lattice oxygen, J. Am. Ceram. Soc. 83 (8) (2000) 1985–1992.
[20] M. Kitayama, K. Hirao, M. Toriyama, S. Kanzaki, Control of beta-Si_3N_4 crystal mophology and its mechanisms (Part 1). Effect of SiO_2 and Y_2O_3 ratio, J. Ceram. Soc. Jpn. 107 (10) (1999) 930–934.
[21] A.J. Moulson, Reaction-bonded silicon nitride: its formation and properties, J. Mater. Sci. 18 (1983) 951–967.
[22] K.H. Ko, K.S. Bang, K.T. Lim, D.S. Park, H.D. Kim, C. Park, Microstructural study of a discoloration process in reaction bonding of silicon nitride, J. Ceram. Process. Res. 8 (3) (2007) 199–202.
[23] I.C. Jung, S.H. Cho, S.W. Na, J. Lee, H.S. Lee, W.S. Cho, Synthesis of Si_3N_4 whiskers in porous SiC bodies, Mater. Lett. 61 (2007) 4843–4846.